Acta Materialia 125 (2017) 296–302

Contents lists available at ScienceDirect

Acta Materialia

journal homepage: www.elsevier.com/locate/actamat

Full length article

Large recovery of six-fold twinned nanowires of α-Fe

Suzhi Li [a, *], Ekhard K.H. Salje [a, b], Sun Jun [a], Xiangdong Ding [a, **]

[a] State Key Laboratory for Mechanical Behavior of Materials, Xi'an Jiaotong University, Xi'an 710049, China
[b] Department of Earth Sciences, University of Cambridge, Cambridge CB2 3EQ, UK

ARTICLE INFO

Article history:
Received 9 August 2016
Received in revised form
26 November 2016
Accepted 3 December 2016
Available online 19 December 2016

Keywords:
Six-fold twinning
Torsion
Pseudo-elasticity
α-Fe nanowire
Avalanches

ABSTRACT

Six-fold twinned nanowires sustain very large twists under torsion. The twist is generated by mobile twin boundaries. In contrast, torsion in un-twinned nanowires is carried by dislocations and leads to failure for small torsion angles. The twisted, twinned nanowire can be totally "untwisted" by the reverse motion of twin boundaries, leading to huge pseudo-elasticity. The movement of twin boundaries and dislocations is non-smooth. It progresses by jerks and avalanches. Molecular dynamics simulations show that twin boundary jerks are power law distributed and the size exponent is compatible with mean field theory.

1. Introduction

The driving force of shape recovery in traditional shape memory alloys (SMAs) arises from the free energy difference between the martensite and austenite phases [1–3]. The effect is strongly size-dependent and it is not obvious how SMAs operate in nano-objects [4,5]. We know that many nano-scale SMAs fail and break [6] so that it becomes important to develop alternative functional materials, which can replace SMAs in nano-devices. These alternative materials are often themselves not SMAs but nevertheless show pseudo-elasticity or shape memory effect (SME) such as shape recovery under mechanical forcing. Typical examples are nanowires with face-centered-cubic (fcc) and body-centered-cubic (bcc) structures, which sustain pseudo-elasticity under reversible deformation by reversible twinning [7–10]. While these twinning effects were reported mostly for tension and shear deformation of nanowires in α-Fe, nothing is known about torsion, which is expected to be the main deformation mode in nano-devices, such as nano-spring [11], torsional oscillator [12] and torsional actuator [13] etc. Here we show that twin boundary (TB) movements in α-Fe nanowires lead indeed to high quality pseudo-elasticity.

SME depends strongly on the nano-structure of the wire. Shape changes in pristine α-Fe wires are small and torsion is difficult to achieve. This situation changes dramatically when the wire is twinned. Twinning along the torsional wire axis may increase the reversible torsion angle dramatically. This massive increase is a property of twin boundaries and the elastic softness of twinned structures and has nothing to do with the bulk crystal structure [14], only twinning dominates the pseudo-elasticity and SME [2]. Furthermore, the interactions of twin boundaries with defects influences mechanical properties when twin boundary act as barriers for dislocation motion [15,16]. The predominance of twinning is equally seen in electrical and magnetic properties, which also behave quite differently near twin boundaries. For example, twin walls are polar while the bulk is non-polar in $CaTiO_3$ [17] and are superconducting in insulating WO_{3-x} [18]. Twin boundaries were seen before in nanowires: twinned superlattices were found in II–V semiconductors indium phosphide [19], in nanowires grown on silicon (111) planes [20], high densities of twin boundaries and stacking faults were found in ultrathin gold-copper nanowires [21], in nano-twinned silver nanowires [22] and during wire growth nucleated by twin boundaries in CuO [23]. These twin boundaries greatly influence the mechanical properties of the nanowire under torsion. In this paper we predict the twinning laws and torsion properties in α-Fe using molecular dynamics (MD) simulations.

The twin system of α-Fe is <111>/{112}. We report the effect of two twin configurations, which influence the torsion-induced pseudo-elasticity most profoundly, with twin boundaries along the trigonal torsional axis [111] (Fig. 1). The two configurations

* Corresponding author.
** Corresponding author.
E-mail addresses: lsuzhi@gmail.com (S. Li), dingxd@mail.xjtu.edu.cn (X. Ding).

http://dx.doi.org/10.1016/j.actamat.2016.12.002
1359-6454/

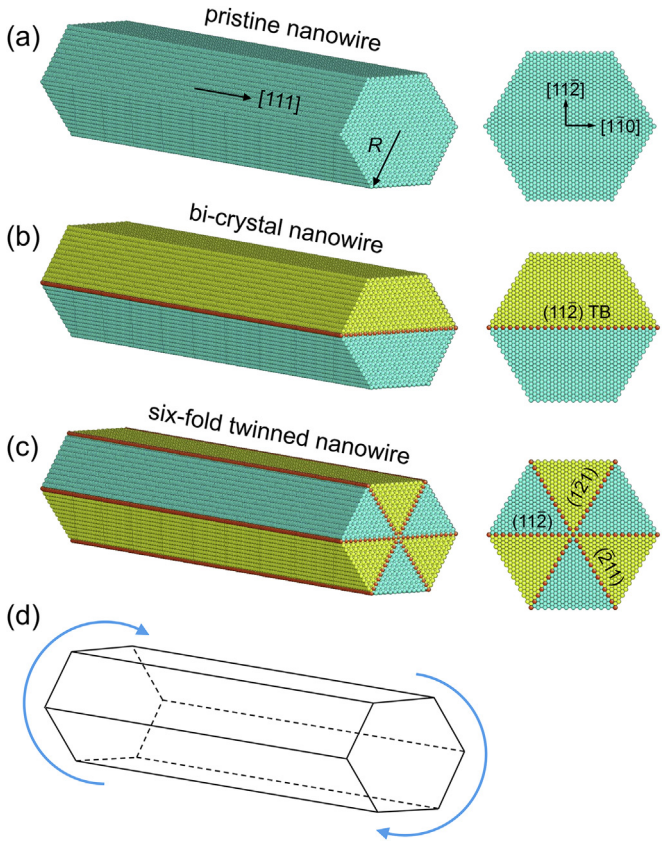

Fig. 1. Illustration of six-fold twinned structure in [111]-oriented bcc nanowires. (a) A pristine nanowire. (b) A bi-crystal nanowire with a preexisting [111]/(11$\bar{2}$) twin boundary. (c) A six-fold twinning nanowire with three equivalent {112} planes as the twinning planes. (d) Model of applying torsion to nanowires.

consist of either one twin boundary or three twin boundaries. Both configurations are compatible with the symmetry of the crystal. We then twist the sample around the [111] axis and identify the recoverable torsion SME.

2. Simulation methods

Starting from a [111]-oriented pristine nanowire (Fig. 1a), a bi-crystal is created by the (11$\bar{2}$) plane as the mirror plane (Fig. 1b). This <111>/{112}-type twin is the typical twin structure in bcc metals. The two twin domains are oriented as x-[1$\bar{1}$0], y-[11$\bar{2}$], z-[111] and x-[$\bar{1}$10], y-[$\bar{1}\bar{1}$2], z-[111]. There are three crystallographically equivalent {112} planes. Each two equivalent {112} planes have an intersection angle of 60°. Therefore, we can further create the six-fold twin structure by taking each {112} plane as a twin boundary. Fig. 1c shows the three twin boundaries with 60° interstitial angle. The three twin boundaries divided the crystal into six domains with two different orientations as shown in two different colors in Fig. 1c. Unlike the reported five-fold twinning in fcc crystal [24,25], where disclinations are required to connect the domain misfit, here the domains in bcc crystals could construct the six-fold twinned structure without any volume compensation.

Atomic interactions of α-Fe are described by the embedded atom method (EAM) developed by Mendelev et al. (potential #4) [26]. Various properties, such as the elastic constants, point defect energy, low-index surface energy etc., predicted by this potential are in good agreement with data obtained by experiments or first-principles calculations. To perform torsion, the nanowire was first relaxed at 50 K for one nanosecond using the Nosé-Hoover thermostat [27,28]. Then several atomic layers at two ends of the nanowire were fixed rigidly as the loading grip. The torsion was applied by rotating the rigid loading ends around the long axis of the nanowire (Fig. 1d). The twist was applied with a rate of 0.2° per picosecond. Unloading was performed in a similar way by rotating the grip in the opposite direction. To study the size effect, we fixed the length of nanowires first to be 65.3 nm and changed the wire radius R into a series of values ranging from 2.4 nm to 4.8 nm. The torsion was applied with the same twist rate. We also used another EAM (potential #2) [26] to check our simulation results. Similar results were obtained by using both potentials. All the MD calculations were carried out by using the LAMMPS code [29]. The atomic configurations were displayed by AtomEye [30].

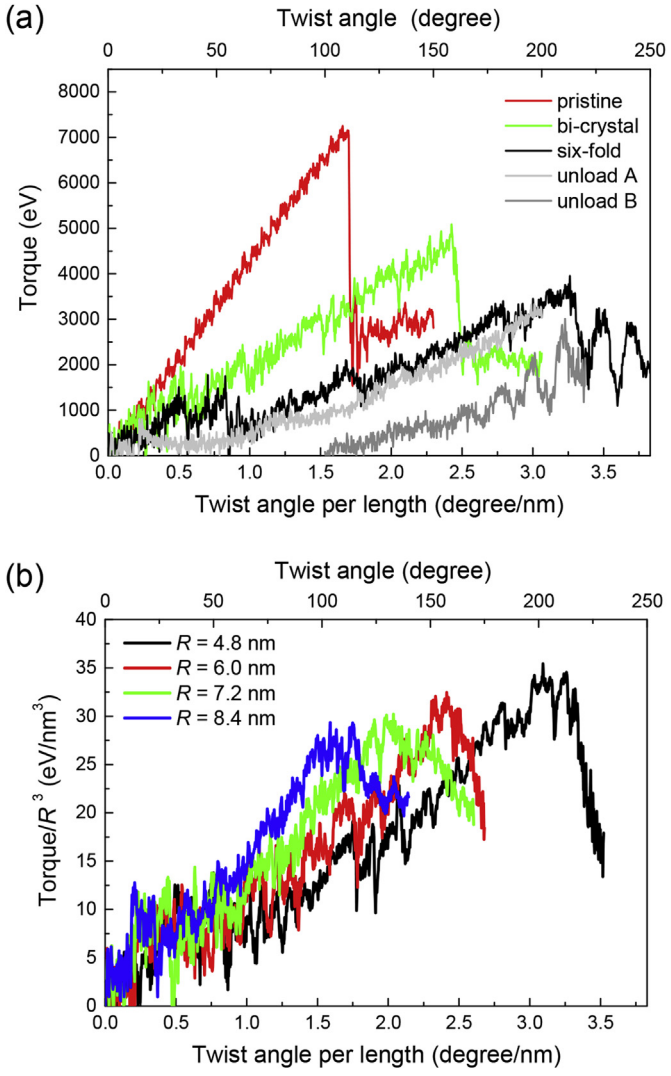

Fig. 2. (a) The variation of torque with twist angle per length (and twist angle) for pristine (red), bi-crystal (green) and six-fold twinned (black) nanowires for $R = 4.8$ nm. Two stages are selected to unload the six-fold twinned nanowires as path A (light grey) and path B (dark grey), respectively. (b) The variation of torque with twist angle for different sized nanowires. The black, red, green and blue curves correspond to $R = 4.8$ nm, 6.0 nm, 7.2 nm and 8.4 nm, respectively. (For interpretation of the references to colour in this figure legend, the reader is referred to the web version of this article.)

3. Results and discussion

3.1. Torsion deformation in different types of nanowires

Torsion generates the shear stress in the cross-section as $\tau = Tr/J$, where T is the applied torque, r is the radius and J is the polar moment of inertia. J is calculated as the integral over r^2 in the cross-sectional area A as $\int_A r^2 dA$ and depends on the fourth power of the radius (Fig. 1d). This torsion on six-fold twinned nanowires is compared with the same tests in the pristine and bi-crystal nanowires. Fig. 2a shows the variation of torque as the function of applied twist angle per length (and twist angle ϕ) for the three nanowires. For the pristine nanowire, the torque increases linearly in the elastic regime and then undergoes a sudden drop at the yield point. The elastic deformation increases for twist angles until $\phi = 110^\circ$. The torque then remains at a low value under further twist. The torque mechanism in bi-crystal and six-fold twinned nanowires are very different. The yield occurs at a lower angle. After yield, the flow stress does not drop, but exhibits the mechanical strengthening so that the torque continues to increase under further loading. The six-fold twinned nanowire has a weaker strengthening than the bi-crystal due to the larger number of TBs. The strengthening lasts for $\phi = 160^\circ$ in bi-crystal nanowire and $\phi = 210^\circ$ in six-fold twinned nanowires. After strengthening, the torque undergoes a sudden drop with the value remaining at a lower level under further twist.

We selected two states to unload the nanowire to test the shape recovery [7,8,31]. One is close to the termination of the strengthening stage at $\phi = 200^\circ$ (path A) and the other is the one right after the strengthen stage $\phi = 220^\circ$ (path B) (Fig. 2a). We find the unloading torque follows the loading curve for path A, which defines pseudo-elasticity. This is different from the loading curve B where the torque disappears when the twist angle reaches ca.100°. The nanowire cannot fully recovery when the maximum torque exceeds the strength limit.

The simulations were designed to identify shape recovery under torsion in nanowires. When increasing the diameter of the nanowire we expect a decrease of the recoverable toque. The torque is expressed as effective stress [32] by torque divided by the R^3, which removes the explicit dependence of the recovery curves on the wire radius. Fig. 2b shows the variation of effective shear stress as the function of twist angle per length for different sized nanowires (R = 4.8 nm, 6.0 nm, 7.2 nm and 8.4 nm). As R increases, the strengthening effect becomes much stronger. Therefore, the effective stress reaches the critical value for large stress drop at much

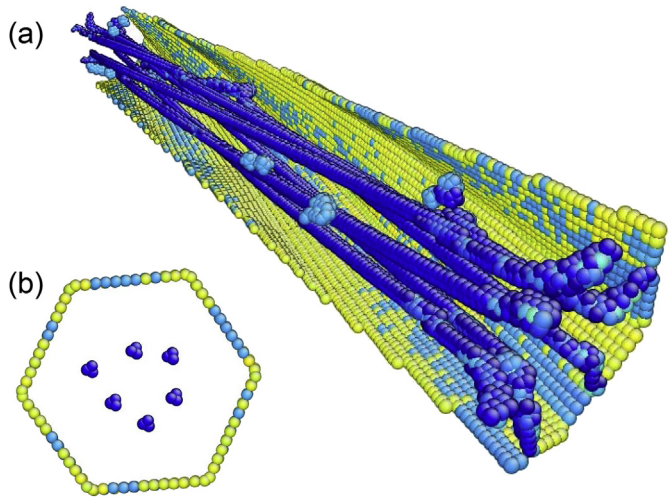

Fig. 4. Dislocation pattern in pristine nanowires. (a) The nanowire is cut to present a good view to dislocation configurations. (b) Cross-sectional view of dislocation pattern. The six screw dislocations arrange symmetrically. The color is shown according to the centro-symmetry parameter [45].

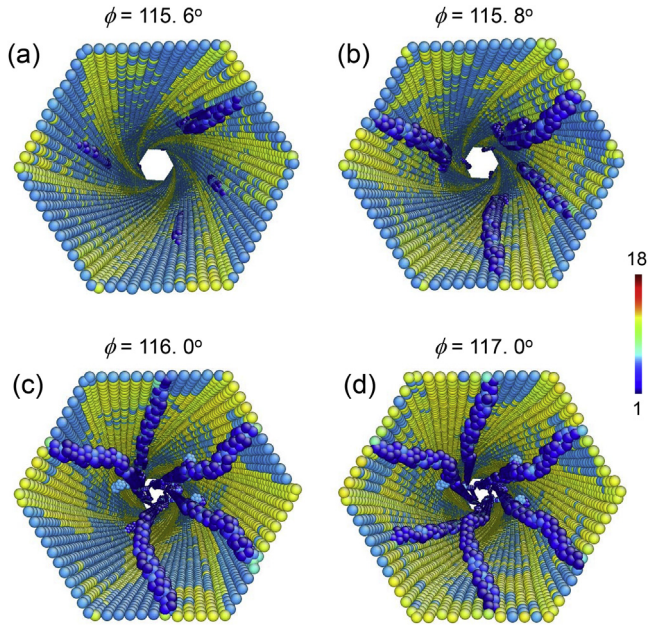

Fig. 3. Typical images of plastic deformation of pristine nanowires. (a) Screw dislocations (in dark blue colors) nucleate at free surfaces of nanowires and (b) move towards the inside of nanowires. (c)–(d) Further loading generates more dislocations. The color is shown according to the centro-symmetry parameter [45]. (For interpretation of the references to colour in this figure legend, the reader is referred to the web version of this article.)

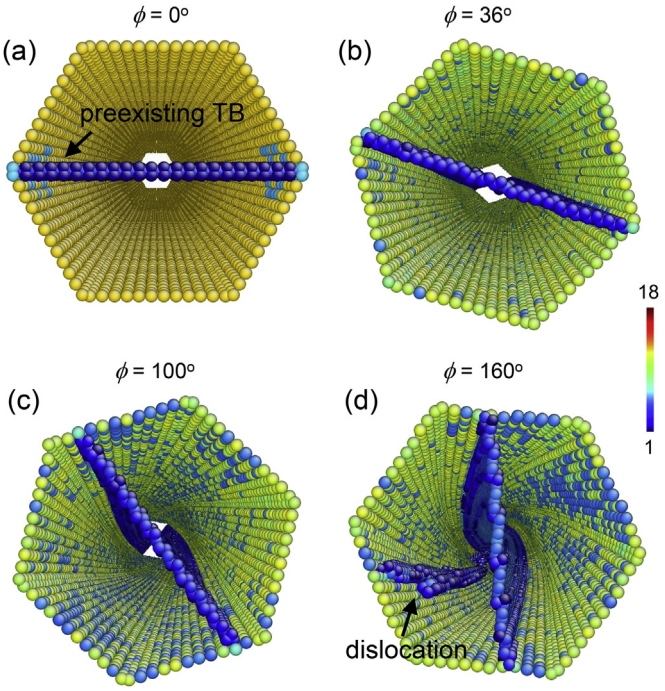

Fig. 5. Typical images of plastic deformation of bi-crystal nanowires. (a) The initial configuration with a preexisting TB. (b) TB starts to move. (c) TB is further twisted. (d) Screw dislocations are finally generated. The color is shown according to the centro-symmetry parameter [45].

lower twisting angle. The yield points for various R are almost identical in the T/R^3, which is reached for greater R at lower twist angles. The torsion-induced pseudo-elasticity shows hence a strong size effect that the recoverable twist angle decreases as the wire diameter increases.

3.2. Deformation mechanisms

The atomic configuration of the un-twinned nanowire contains a multitude of dislocations (Fig. 3). When the sample yields at $\phi = 115.6°$, screw dislocations are firstly nucleated from the free surfaces and driven towards the inside of the nanowires. Further loading generates more dislocations. Finally, there are six dislocations with each one generated in one free surface. Fig. 4a shows a snapshot of the dislocation configuration with screw dislocations undergoing slip. Dislocation interactions and dislocation motion can generate point defects [33]. There are also some point defects left during the movement of screw dislocations. Six dislocations finally form a stable pattern (Fig. 4b) with a symmetrical arrangement, similar to that in gold nanowires [34].

Typical atomic images during twisting of a twinned nanowire show that plastic strain is carried by TB motion. Instead of dislocations, the twin boundary motion dominates during the whole strengthening stage, as the bi-crystal shown in Fig. 5. When the twisting angle is very large, the single TB itself cannot sustain such large rotation and dislocations are generated at around $\phi = 160°$ (after the strengthening stage). Owing to the different loading orientation, there is no detwinning as that occurs in fcc nanowires [35]. Fig. 6 shows the typical images during the loading/unloading of the six-fold twinned nanowire. Starting from a nanowire with three preexisting TBs (Fig. 6a), the sample can undergo a twist of ca. 210°, which is much larger than that in bi-crystal. The steady state strengthening corresponds to the collective motion of all three TBs (Fig. 6b). The exhaustion of TB motion comes with the emission of dislocations (Fig. 6c), which corresponds to a drop of torque in Fig. 2a. The unloading before the dislocation emission can make the nanowire in a good shape recovery (Fig. 6d). However, once the dislocations are generated, the nanowire can only recover partially upon unloading (Fig. 6e).

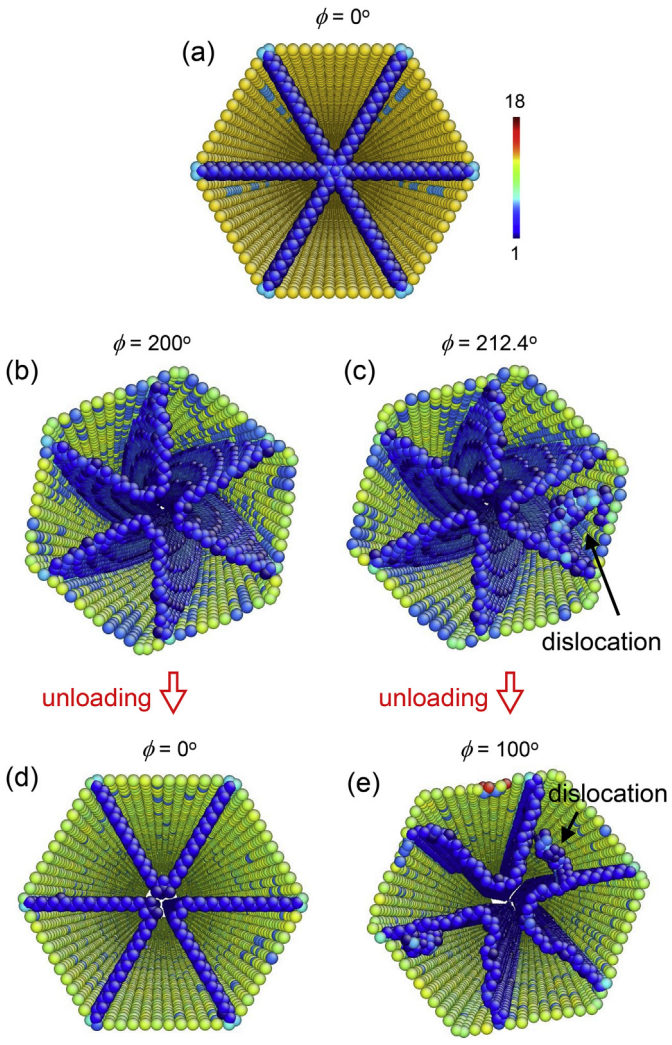

Fig. 6. Typical images of plastic deformation of six-fold twinned nanowires. (a) The initial configuration with three equivalent preexisting TBs. (b) TB is severely twisted. (c) Dislocations are finally generated. (d) Unloading at state $\phi = 200°$. (e) Unloading at state $\phi = 212.4°$. The color is shown according to the centro-symmetry parameter [45].

For the role of twin boundary on the mechanical performance, these preexisting planar defects can make the nanowires yield at low twisting angle when comparing to that of pristine nanowires since the twin boundary only requires a smaller stress to move. The more twin boundaries added, the lower yielding point. After yielding, we can see an obvious strengthening in a large plastic regime in the twinned nanowires, quite different to that in pristine nanowires. The reason lies in that the twisted twin boundary can increase the deformation energy gradually, which produces the observed strengthening.

Our simulation results show that the yielding stress has a weak dependence on the wire diameter in six-fold twinned nanowires (Fig. 2b). We know that the yielding corresponds to the motion of preexisting twin boundaries, not to the nucleation of new defects, such as the dislocations generation. In our earlier work [7], we calculated the energy landscape for twinning deformation in bcc crystals in terms of generalized stacking faults energy. These results showed that the nucleation of twin layers required a much higher energy than the energy barrier for subsequent twin motion (or growth) [7]. Thus, with regard to the preset twin boundaries in the nanowire, we can expect they are driven at a similar stress level, leading to a weak dependence on wire size, as shown in Fig. 2b.

It is noted that, when we compare the magnitude of torque for generating dislocations for the three kinds of nanowires, we find that the dislocations require a high torque in pristine nanowires but a lower torque in six-fold twinned nanowires. The reason might lie in that the twin boundaries produce stress fields, which nucleate dislocations at low torque. Fig. 7 shows the interactions between dislocations and twin boundaries in the six-fold twinned nanowires. The dislocations are generated at extremely larger twisting angle ($\phi > 210°$). These dislocations first nucleate in the surfaces near the rigid loading grip (Fig. 7a). Once nucleated, they move towards the core region. When they meet the twin boundaries, they cannot penetrate the twin boundary to move further but are stored in the sub-grains (Fig. 7b). Further torsion can generate more dislocations in other sub-grains (Fig. 7c). These dislocations are all accumulated and localized the plastic deformation (Fig. 7d). Finally, necking occurs in this site which induces the permanent irreversible deformation to the nanowires.

3.3. Energy analysis

Pseudo-elastic behavior of nanowires under tension is driven by the reduction of the surface energy [9,10,31]. The large surface energy in nanowires can even induce spontaneous crystal reorientation [36] or inverse phase transition [37]. We compare this surface-energy-driven mechanism with the torsion-induced pseudo-elasticity. The potential energy changes during the

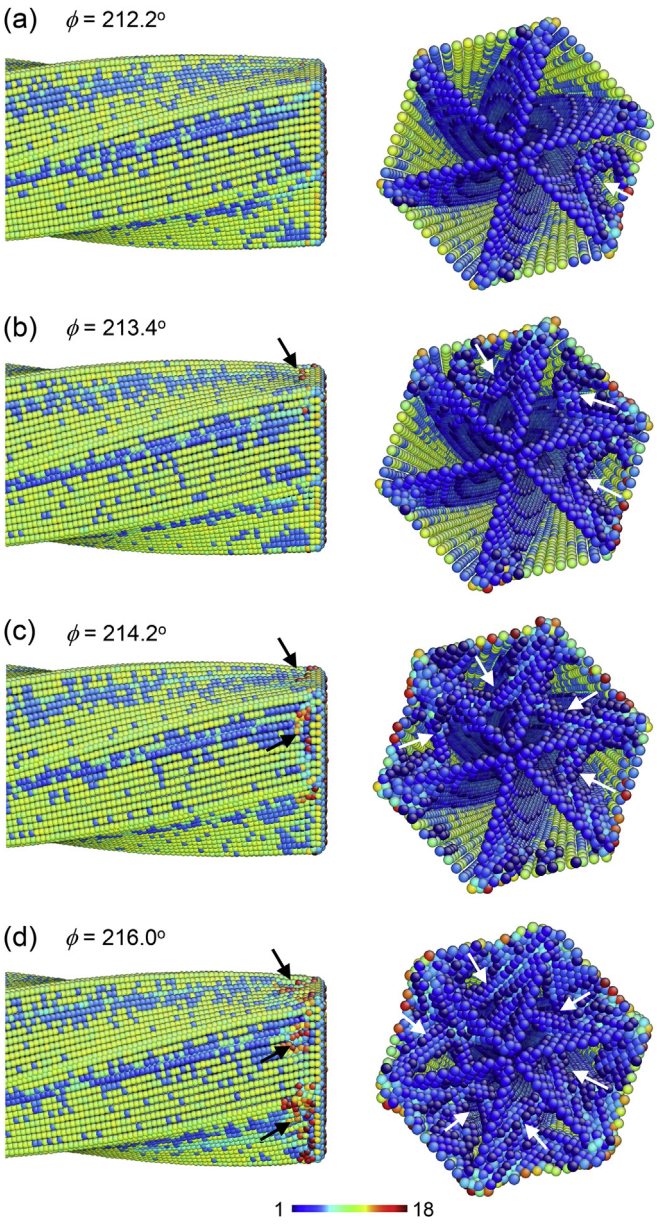

Fig. 7. Several snapshots for the interactions between dislocations and twin boundaries at different twisting angle in six-fold twinned nanowires. The left column shows the side-view images in the section of nanowires at the end. The right column shows the images when viewing along the axis of nanowire. (a) The dislocations first nucleate in the surfaces around the rigid loading grip, as the white arrows indicate. (b) When dislocations meet twin boundaries, they cannot penetrate the boundary but are stored in the sub-grain. (c) Further torsion can generate more dislocations. (d) With more dislocations are induced, the deformation is concentrated in the local area, roughening the surfaces, as the black arrows indicate. The color is shown according to the centro-symmetry parameter [45].

deformation process, with three contributions identifiable: the surface energy change (ΔE_{surf}), the deformation of twin boundary energy (ΔE_{TB}), and the stored bulk elastic energy ($\Delta E_{bulk\text{-}ela}$). We calculate each component ΔE_{surf}, ΔE_{TB} and $\Delta E_{bulk\text{-}ela}$ under loading/unloading to identify their contribution to pseudoelasticity. We use the same criterion in terms of distribution of atomic potential energy (E_{pot}^{atom}) to distinguish the different groups of energy components atom-by-atom as in Ref. [8]. Let us take $\phi = 50^{\circ}$ as an example (Fig. 8a). We define atoms in the outermost three layers as the surface layers, which can take account for 99% of the surface energy. In the bulk there is an overlap between the bulk elastic energy and the twin boundary energy. The overlap comes from those atoms further away from the core region of twin boundaries, which will approach the bulk energy. Fig. 8b shows the normalized distribution of E_{pot}^{atom} for all the atoms outside the surface layers. There is a peak in the low energy region and an asymmetric distribution for higher energies. The peak corresponds to the bulk elastic energy while the asymmetric shoulder corresponds to the twin boundary regime. To distinguish the two energy components, we define a threshold value. Assuming the distribution of bulk elastic energy follows a normal distribution at finite temperature (data in black color). We find that a large deviation occurs when E_{pot}^{atom} is around −4.10 eV. This value was taken as the threshold to separate bulk elastic energy and twin boundary energy. The atoms with E_{pot}^{atom} smaller than the threshold are considered as bulk, larger values as twin boundary atoms.

Fig. 8c shows the variation of all the energy components in the loading and unloading stages. The energy component is further averaged to the corresponding number of atoms in each group as $\Delta E_{bulk\text{-}ela}{}^{atom}$, $\Delta E_{surf}{}^{atom}$ and $\Delta E_{TB}{}^{atom}$. The three components increase continuously during loading. There is a jump for $\Delta E_{surf}{}^{atom}$ and $\Delta E_{TB}{}^{atom}$ and an obvious drop for $\Delta E_{bulk\text{-}ela}{}^{atom}$ when entering the plastic regime. At higher loading, $\Delta E_{TB}{}^{atom}$ remains almost constant while $\Delta E_{bulk\text{-}ela}{}^{atom}$ and $\Delta E_{surf}{}^{atom}$ increase gradually; $\Delta E_{surf}{}^{atom}$ increases more strongly than $\Delta E_{bulk\text{-}ela}{}^{atom}$. There are some local jumps in $\Delta E_{surf}{}^{atom}$, which may be due to the sluggish motion of twin boundaries at low temperature. These local jumps are also seen in torque-angle curves (Fig. 2a). Upon unloading, the components $\Delta E_{bulk\text{-}ela}{}^{atom}$ and $\Delta E_{surf}{}^{atom}$ decrease gradually, but $\Delta E_{TB}{}^{atom}$ still exhibits a long plateau with the magnitude almost unchanged until it decreases at the end of the unloading stage.

This analysis shows that the stored bulk elastic energy and surface energy provide the driving force of shape recovery. Unlike in tension-induced pseudo-elasticity [9,10,31] where the surface energy is altered by crystal reorientation, the change of surface energy is mostly from the elastic twisting of surfaces under torsion. Therefore, in a general sense, $\Delta E_{surf}{}^{atom}$ could also be classified as elastic energy change, but distinguished from bulk elastic energy $\Delta E_{bulk\text{-}ela}{}^{atom}$.

3.4. Avalanche dynamics

The evolution of the torsion movement is not a smooth function of time. Under torsion, the twin boundaries rotation is jerky. Similarly, the nucleation of dislocation also occurs in a stepwise manner. Such “jerky” time evolution is often characterized by avalanche processes where each small advance can trigger a multitude of secondary processes. The avalanche dynamics in wires and disordered materials was reviewed in Ref. [38]. The hallmark of avalanche dynamics is the power law distribution of the “jerks” with power law exponents from within a small range of parameters. We tested this hypothesis in our twinned systems and found that the jerk distribution is indeed power-law distributed (see Fig. 9). The linear log-log distribution shows a power law range of one decade. This value is limited by the statistics of the MD simulations where the short time scale and rapid superposition for avalanches disallows for large scale distributions [39]. The slope of the logarithmic probability distribution functions is near 1.5 and hence compatible with the predicted values of mean field theory [31], which is close to values observed for slip in nano-materials [40]. Sheared nano-pillars were found to slip with similar exponents [33].

We also tested the avalanche dynamics for finite size effects but found no evidence despite the small diameter of the wire (see Fig. 9). The absence of finite size scaling appears to imply that the relevant length scale for the jerky movement is below 4.8 nm and hence extends over only few interatomic distances.

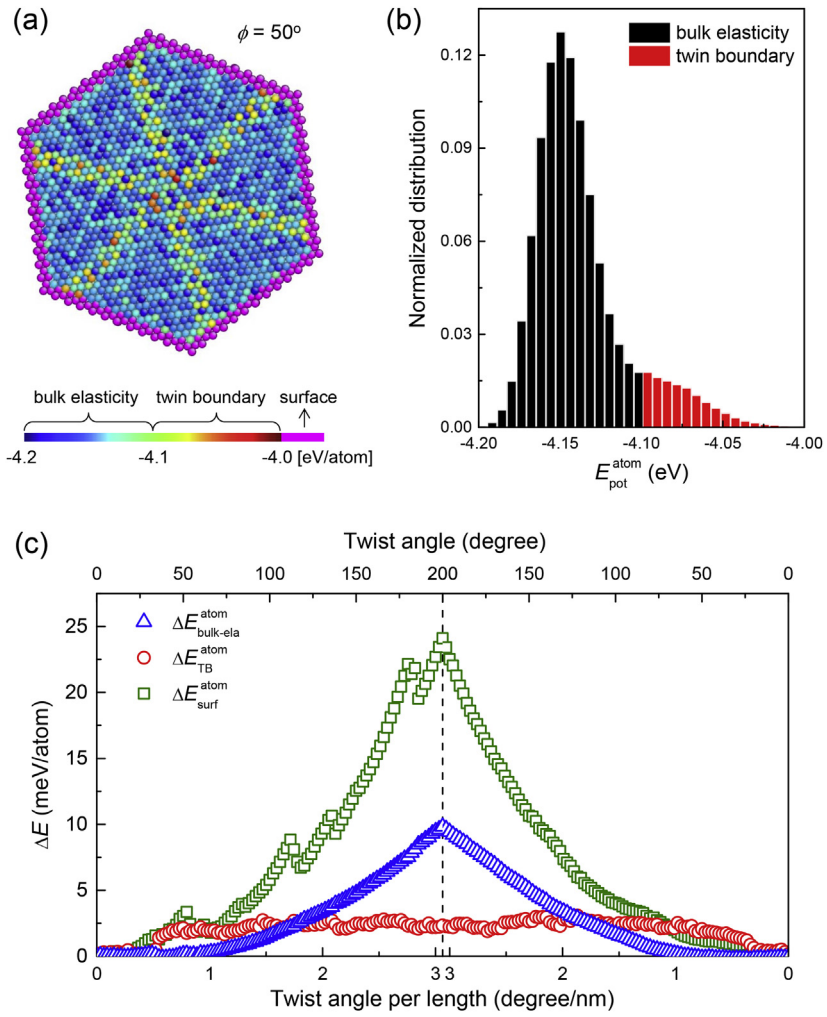

Fig. 8. (a) Distribution of atomic potential energy (E_{pot}^{atom}) in a twisted nanowire at $\phi = 50°$. (b) The histogram of E_{pot}^{atom} distribution for atoms in regime of bulk elasticity (black) and twin boundaries (red). (c) Variation of energy components upon loading and unloading. Blue triangle, red circle and green square represent $\Delta E_{bulk\text{-}ela}^{atom}$, ΔE_{TB}^{atom} and ΔE_{surf}^{atom}, separately. (For interpretation of the references to colour in this figure legend, the reader is referred to the web version of this article.)

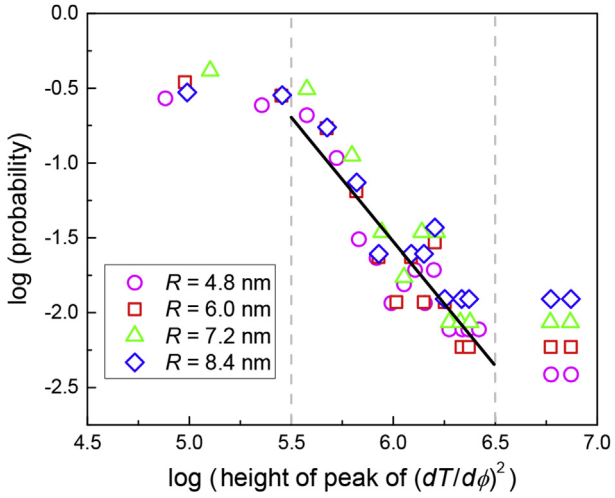

Fig. 9. (a) log-log plot of probability of the peaks of $(dT/d\phi)^2$ for six-fold twinned nanowires in different size. Linear fitting was made for the values in range of [5.5, 6.5]. The slopes are −1.59, −1.80, −1.89 and −1.47 for R = 4.8 nm, 6.0 nm, 7.2 nm and 8.4 nm, respectively.

3.5. Experimental observations

Only few experimental results have been obtained for torsion experiments on nanowires that may be correlated with our results. Hodge et al. [41] studied the twin stability of nano-twinned Cu upon high pressure torsion (HPT) and found that the original columns of twins in the interiors of samples persist to high shear strains. Other experiments show that the deformed twin show good recovery under torsion in Mg–Al–Zr alloys [42]. Hardening was found for the large densities of twins in Co [43]. Nano-grained NiTi shape memory alloy also exhibit monotonic hardening upon torsion [44]. In none of these experiments we find nano-twinned configurations so that large angle torsion could not yet be observed. Nevertheless, once a suitably twinned nanowire has been produced we expect high torsional flexibility.

4. Conclusions

By using molecular dynamics simulations, we studied the mechanical deformation of six-fold twinned nanowires upon twisting. Unlike the pristine nanowires where the plastic strain is primarily carried by dislocations, the six-fold twinned nanowires undergo severely twisting with the aid of TBs motion before dislocations are

generated. The twisted nanowires can be fully recovered upon unloading, leading to a novel pseudo-elastic behavior. The twin boundary motion is non-smooth, but proceeds by jerks. The present work enriches potential applications of twinned nanowires as the functional devices.

Acknowledgements

XD and JS appreciate the support of NSFC (51231008, 51320105014, 51621063), the 973 Programs of China (2012CB619402). EKHS is grateful to the Leverhulme trust (EM-2016-004) and EPSRC (EP/K009702/1).

References

[1] K. Otsuka, X. Ren, Physical metallurgy of Ti-Ni-based shape memory alloys, Prog. Mater. Sci. 50 (5) (2005) 511–678.
[2] X. Ding, T. Suzuki, X. Ren, J. Sun, K. Otsuka, Precursors to stress-induced martensitic transformations and associated superelasticity: molecular dynamics simulations and an analytical theory, Phys. Rev. B 74 (10) (2006) 104111.
[3] A. Planes, L. Manosa, Vibrational properties of shape-memory alloys, Solid State Phys. 55 (2001) 159–267.
[4] Y.Q. Fu, S. Zhang, M.J. Wu, W.M. Huang, H.J. Du, J.K. Luo, A.J. Flewitt, W.I. Milne, On the lower thickness boundary of sputtered TiNi films for shape memory application, Thin Solid Films 515 (1) (2006) 80–86.
[5] T. Waitz, T. Antretter, F.D. Fischer, N.K. Simha, H.P. Karnthaler, Size effects on the martensitic phase transformation of NiTi nanograins, J. Mech. Phys. Solids 55 (2) (2007) 419–444.
[6] L. Liu, X. Ding, J. Sun, S. Li, E.K.H. Salje, Breakdown of shape memory effect in bent Cu–Al–Ni nanopillars: when twin boundaries become stacking faults, Nano Lett. 16 (1) (2015) 194–198.
[7] S. Li, X. Ding, J. Deng, T. Lookman, J. Li, X. Ren, J. Sun, A. Saxena, Superelasticity in bcc nanowires by a reversible twinning mechanism, Phys. Rev. B 82 (20) (2010) 205435.
[8] Y. Yang, S. Li, X. Ding, J. Sun, E.K.H. Salje, Interface driven pseudo-elasticity in α-Fe nanowires, Adv. Funct. Mater. 26 (5) (2016) 760–767.
[9] W. Liang, M. Zhou, F. Ke, Shape memory effect in Cu nanowires, Nano Lett. 5 (10) (2005) 2039–2043.
[10] H.S. Park, K. Gall, J.A. Zimmerman, Shape memory and pseudoelasticity in metal nanowires, Phys. Rev. Lett. 95 (25) (2005) 255504.
[11] A.F. da Fonseca, D.S. Galvão, Mechanical properties of nanosprings, Phys. Rev. Lett. 92 (17) (2004) 175502.
[12] S. Evoy, D. Carr, L. Sekaric, A. Olkhovets, J. Parpia, H. Craighead, Nanofabrication and electrostatic operation of single-crystal silicon paddle oscillators, J. Appl. Phys. 86 (11) (1999) 6072–6077.
[13] J. Hsieh, W. Fang, A novel microelectrostatic torsional actuator, Sens. Actuators A Phys. 79 (1) (2000) 64–70.
[14] L. Goncalves-Ferreira, S.A.T. Redfern, E. Atacho, E.K.H. Salje, The intrinsic elasticity of twin walls: ferrielectric twin walls in ferroelastic $CaTiO_3$, Appl. Phys. Lett. 94 (8) (2009).
[15] T. Zhu, J. Li, A. Samanta, H.G. Kim, S. Suresh, Interfacial plasticity governs strain rate sensitivity and ductility in nanostructured metals, PNAS 104 (9) (2007) 3031–3036.
[16] K. Lu, L. Lu, S. Suresh, Strengthening materials by engineering coherent internal boundaries at the nanoscale, Science 324 (5925) (2009) 349–352.
[17] S. Van Aert, S. Turner, R. Delville, D. Schryvers, G. Van Tendeloo, E.K.H. Salje, Direct observation of ferrielectricity at ferroelastic domain boundaries in $CaTiO_3$ by electron microscopy, Adv. Mater. 24 (4) (2012) 523–527.
[18] A. Aird, E.K.H. Salje, Sheet superconductivity in twin walls: experimental evidence of, J. Phys. Condens. Matter 10 (22) (1998) L377.
[19] X. Qihua, J. Wang, P.C. Eklund, Coherent twinning phenomena: towards twinning superlattices in III-V semiconducting nanowires, Nano Lett. 6 (12) (2006) 2736–2742.
[20] R.L. Woo, R. Xiao, Y. Kobayashi, L. Gao, N. Goel, M.K. Hudait, T.E. Mallouk, R.F. Hicks, Effect of twinning on the photoluminescence and photoelectrochemical properties of indium phosphide nanowires grown on silicon (111), Nano Lett. 8 (12) (2008) 4664–4669.
[21] R. Mendoza-Cruz, L. Bazan-Diaz, J.J. Velazquez-Salazar, G. Plascencia-Villa, D. Bahena-Uribe, J. Reyes-Gasga, D. Romeu, G. Guisbiers, R. Herrera-Becerra, M. Jose-Yacaman, Helical growth of ultrathin gold-copper nanowires, Nano Lett. 16 (3) (2016) 1568–1573.
[22] A. Kobler, T. Beuth, T. Kloeffel, R. Prang, M. Moosmann, T. Seherer, S. Walheim, H. Hahn, C. Kuebel, B. Meyer, T. Schimmel, E. Bitzek, Nanotwinned silver nanowires: structure and mechanical properties, Acta Mater. 92 (2015) 299–308.
[23] S. Rackauskas, H. Jiang, J.B. Wagner, S.D. Shandakov, T.W. Hansen, E.I. Kauppinen, A.G. Nasibulin, In situ study of noncatalytic metal oxide nanowire growth, Nano Lett. 14 (10) (2014) 5810–5813.
[24] J. Wu, S. Nagao, J. He, Z. Zhang, Role of five-fold twin boundary on the enhanced mechanical properties of fcc Fe nanowires, Nano Lett. 11 (12) (2011) 5264–5273.
[25] Q. Qin, S. Yin, G. Cheng, X. Li, T.-H. Chang, G. Richter, Y. Zhu, H. Gao, Recoverable plasticity in penta-twinned metallic nanowires governed by dislocation nucleation and retraction, Nat. Commun. 6 (2015).
[26] M. Mendelev, S. Han, D. Srolovitz, G. Ackland, D. Sun, M. Asta, Development of new interatomic potentials appropriate for crystalline and liquid iron, Philos. Mag. 83 (35) (2003) 3977–3994.
[27] S. Nosé, A unified formulation of the constant temperature molecular dynamics methods, J. Chem. Phys. 81 (1) (1984) 511–519.
[28] W.G. Hoover, Canonical dynamics - equilibrium phase-space distributions, Phys. Rev. A 31 (3) (1985) 1695–1697.
[29] S. Plimpton, Fast parallel algorithms for short-range molecular dynamics, J. Comput. Phys. 117 (1) (1995) 1–19.
[30] J. Li, AtomEye: an efficient atomistic configuration viewer, Model. Simul. Mater. Sci. Eng. 11 (2) (2003) 173–177.
[31] S. Li, X. Ding, J. Li, X. Ren, J. Sun, E. Ma, High-efficiency mechanical energy storage and retrieval using interfaces in nanowires, Nano Lett. 10 (5) (2010) 1774–1779.
[32] C.R. Weinberger, W. Cai, Plasticity of metal wires in torsion: molecular dynamics and dislocation dynamics simulations, J. Mech. Phys. Solids 58 (7) (2010) 1011–1025.
[33] S. Li, Y. Li, Y.-C. Lo, T. Neeraj, R. Srinivasan, X. Ding, J. Sun, L. Qi, P. Gumbsch, J. Li, The interaction of dislocations and hydrogen-vacancy complexes and its importance for deformation-induced proto nano-voids formation in α-Fe, Int. J. Plast. 74 (2015) 175–191.
[34] C.R. Weinberger, W. Cai, Orientation-dependent plasticity in metal nanowires under torsion: twist boundary formation and Eshelby twist, Nano Lett. 10 (1) (2009) 139–142.
[35] H. Zhou, X. Li, Y. Wang, Z. Liu, W. Yang, H. Gao, Torsional detwinning domino in nanotwinned one-dimensional nanostructures, Nano Lett. 15 (9) (2015) 6082–6087.
[36] J.K. Diao, K. Gall, M.L. Dunn, Surface stress driven reorientation of gold nanowires, Phys. Rev. B 70 (7) (2004) 075413.
[37] S. Li, X. Ding, J. Li, X. Ren, J. Sun, E. Ma, T. Lookman, Inverse martensitic transformation in Zr nanowires, Phys. Rev. B 81 (24) (2010) 245433.
[38] E.K.H. Salje, K.A. Dahmen, Crackling noise in disordered materials, Annu. Rev. Condens. Matter Phys. 5 (1) (2014) 233–254.
[39] E.K.H. Salje, X. Wang, X. Ding, J. Sun, Simulating acoustic emission: the noise of collapsing domains, Phys. Rev. B 90 (6) (2014) 064103.
[40] J. Antonaglia, W.J. Wright, X. Gu, R.R. Byer, T.C. Hufnagel, M. LeBlanc, J.T. Uhl, K.A. Dahmen, Bulk metallic glasses deform via slip avalanches, Phys. Rev. Lett. 112 (15) (2014) 155501.
[41] A. Hodge, T. Furnish, C. Shute, Y. Liao, X. Huang, C. Hong, Y.T. Zhu, T. Barbee Jr., J. Weertman, Twin stability in highly nanotwinned Cu under compression, torsion and tension, Scr. Mater. 66 (11) (2012) 872–877.
[42] M. Myshlyaev, H. McQueen, A. Mwembela, E. Konopleva, Twinning, dynamic recovery and recrystallization in hot worked Mg–Al–Zn alloy, Mater. Sci. Eng. A 337 (1) (2002) 121–133.
[43] J. Sort, A. Zhilyaev, M. Zielinska, J. Nogués, S. Surinach, J. Thibault, M. Baró, Microstructural effects and large microhardness in cobalt processed by high pressure torsion consolidation of ball milled powders, Acta Mater. 51 (20) (2003) 6385–6393.
[44] Q.-P. Sun, Z.-Q. Li, Phase transformation in superelastic NiTi polycrystalline micro-tubes under tension and torsion––from localization to homogeneous deformation, Int. J. Solids Struct. 39 (13) (2002) 3797–3809.
[45] C.L. Kelchner, S. Plimpton, J. Hamilton, Dislocation nucleation and defect structure during surface indentation, Phys. Rev. B 58 (17) (1998) 11085.